PHYSICAL REVIEW B **67**, 094413 (2003)

Inverse tunnel magnetoresistance in all-perovskite junctions of $La_{0.7}Sr_{0.3}MnO_3/SrTiO_3/SrRuO_3$

K. S. Takahashi,[1,2,*] A. Sawa,[1] Y. Ishii,[1] H. Akoh,[1] M. Kawasaki,[1,3] and Y. Tokura[1,2]

[1]*Correlated Electron Research Center (CERC), National Institute of Advanced Industrial Science and Technology (AIST), Tsukuba, Ibaraki 305-8562, Japan*

[2]*Department of Applied Physics, University of Tokyo, Tokyo 113-8656, Japan*

[3]*Institute for Materials Research, Tohoku University, Sendai 980-8577, Japan*

(Received 13 January 2003; published 19 March 2003)

All epitaxial oxide magnetic tunnel junctions, $La_{0.7}Sr_{0.3}MnO_3/SrTiO_3/SrRuO_3$ trilayer films, composed of ferromagnetic and metallic electrodes were fabricated on STO(001) substrates. Inverse tunnel magnetoresistance (TMR), i.e., higher and lower junction resistance levels in parallel and anti-parallel magnetization configurations, respectively, was observed, indicating the negative spin polarization of $SrRuO_3$ in contrast to the positive one of $La_{0.7}Sr_{0.3}MnO_3$. The TMR action persists up to T_C of the $SrRuO_3$ layer due to the robust spin polarization at the $SrTiO_3/SrRuO_3$ interface.

DOI: 10.1103/PhysRevB.67.094413 PACS number(s): 05.45.Df, 05.45.Tp, 72.70.+m

I. INTRODUCTION

Tunnel junctions composed of two ferromagnetic and metallic electrodes separated by an insulating barrier have been attracting considerable attention not only as the probe of the carrier spin polarization but also as the magnetic sensor heads for storage devices and nonvolatile magnetic memories.[1] Large tunnel magnetoresistance (TMR) appears when an applied magnetic field changes the magnetization direction of the two ferromagnetic electrodes. Using Julliere model,[2] the TMR is expressed as

$$\frac{R_{AP}-R_P}{R_P}=\frac{2P_1P_2}{1-P_1P_2}, \qquad (1)$$

where $R_{AP(P)}$ is the junction resistance in the antiparallel (parallel) magnetization state, and P_1 and P_2 are the spin polarizations of two electrodes. The spin polarization P is expressed as

$$P=\frac{N_\uparrow w_\uparrow - N_\downarrow w_\downarrow}{N_\uparrow w_\uparrow + N_\downarrow w_\downarrow}. \qquad (2)$$

Here $N_{\uparrow(\downarrow)}$ is the up (down) -spin density of states (DOS) and $w_{\uparrow(\downarrow)}$ is the weighting factor that can be expressed by square of the averaged Fermi velocity ($v_{\uparrow(\downarrow)}{}^2$) for up (down) -spin electrons in terms of a simple model for the tunneling process.[3]

When the sign of the spin polarization for the two electrodes is opposite to each other ($P_1 \cdot P_2 < 0$), R_P becomes larger than R_{AP}, which we call *inverse* TMR. Recently, Teresa *et al.* reported on the tunnel experiments for Co/I/$La_{0.7}Sr_{0.3}MnO_3$ (LSMO) junctions (I = insulator layer),[4] where the down-spin majority DOS at Fermi level in Co and the up-spin one in LSMO are anticipated to give inverse TMR. Indeed, they observed inverse TMR when I is $SrTiO_3$ (STO) or $Ce_{0.69}La_{0.31}O_{1.845}$, whereas normal TMR emerged for $I = Al_2O_3$. They concluded that the TMR behavior strongly depends on the electronic state at the interface between Co and insulating oxide. There has been also reported an example of unpredictable (whether normal or inverse) TMR for tunnel junctions composed of two Ni-Fe permalloy electrodes depending on the interface chemical state.[5] Thus, it is not straightforward to perform reliable spin-resolved tunneling spectroscopy for junctions using insulating oxide/ferromagnetic metal interface. This is perhaps because the interface oxidation of metallic electrodes and/or the defects at the interface between dissimilar compounds may give rise to additional spin-dependent scattering mechanism. Concerning all-oxide junctions, the inverse TMR for Fe_3O_4 (magnetite)/STO/LSMO was reported, implying the down-spin majority band in Fe_3O_4.[6] Since Fe_3O_4 has spinel type crystal structure and is quite different from perovskite, it seems difficult to control the interface structure on an atomic scale.

Here, we chose $SrRuO_3$ (SRO) and LSMO as electrodes having identical crystal structure of perovskite and opposite spin polarization. Worledge and Geballe have measured the superconducting gap spectrum in a magnetic field for SRO/STO/Al tunnel junction to show that the spin polarization of SRO is negative (-9.5%).[7] Although the value of P is much smaller than the band calculation value ($\sim -60\%$),[8] the negative sign was experimentally confirmed. Therefore, when an all-perovskite tunnel junction is epitaxially composed of SRO and LSMO as the ferromagnetic electrode layers and STO as the barrier layer, it is expected to show inverse TMR due to the opposite sign of spin polarization P, being free from complicated interface phenomena. We have indeed confirmed the inverse magnetoresistance in LSMO/STO/SRO tunnel junctions and investigated the characteristic of spin state and magnetic domains at the interface.

II. EXPERIMENTS

The heteroepitaxial structures were fabricated on STO (001) single-crystal substrates[9] with a pulsed laser deposition system employing KrF excimer laser pulses (100 mJ) focused on polycrystalline targets. During the deposition, the substrate temperature was kept at 800°C under the oxygen pressure of 90 mTorr. The thickness of the LSMO and STO layers was controlled on an atomic scale by *in situ* monitoring the intensity oscillation of reflection high-energy electron

 ©2003 The American Physical Society

diffraction (RHEED),[10] while RHEED oscillation could not be observed for the SRO bottom layer because of the step-flow-type growth mode.[11–13] Instead, we deposited the SRO layer at a constant deposition rate for a prescribed period. The typical trilayer structure is composed of 30-nm-thick SRO bottom electrode/ 8-unit-cells-thick STO barrier layer/ 40-nm-thick LSMO top electrode. After the deposition, the film was cooled in 760 Torr of oxygen. X-ray diffraction was carried out by a four-circle diffractometer with Cu $K\alpha$ source. Magnetization was measured by a superconducting quantum interference device (SQUID) magnetometer. Tunnel junction devices are fabricated by a standard photolithography and ion-milling process.

III. RESULTS AND DISCUSSION

A. Structural characterization

We have performed detailed x-ray diffraction analyses for the heteroepitaxial thin films before the device processing. Figure 1 (a) shows a $2\theta-\theta$ scan of a film composed of LSMO(40 nm)/STO(8 unit cells)/ SRO(30 nm). There can be seen sharp peaks of LSMO (001) and SRO (001) in addition to the STO substrate (001) peak. The full-width of half-maximum of the rocking curve is as narrow as 0.01°. The out-of-plane lattice constants are 0.396 nm for SRO and 0.386 nm for LSMO. The former is elongated from the bulk value of 0.393 nm and the latter is shortened from 0.388 nm. As can be clearly seen in the lower angle tail, Laue interference fringes appear due to the finite thickness of a film. It can be nicely fit as dotted line by assuming the SRO layer thickness to be 30 nm. Therefore, the bottom layer can be concluded to be high crystallinity and extremely flat, the latter of which was also confirmed by atomic force microscope images represented by 0.4 nm steps and atomically flat terraces for SRO single-layer films. Figure 1(b) shows the reciprocal space mapping for the heteroepitaxial thin film. The (114) peaks of SRO and LSMO layers appear at almost the same value of horizontal axis with that of the STO substrate, indicating all the consisting layers have identical in-plane lattice constant to that of the substrate. Therefore, one can expect that there is no dislocation at the interfaces of the tunnel junction. This fact makes us free from being bothered by the issues of interface spin-flipping scattering due to the dislocations at the interfaces. Here we note that the LSMO layer is under tensile strain so that the spin-canting toward *A*-type antiferromagnetic spin ordering may appear at the LSMO/STO interface.[14] This should make spin polarization of LSMO reduced from 100%. The compressive strain of the SRO layer makes the easy magnetization axis to be vertical to the film plane due to spin-orbital coupling.[15] Since TMR response discussed below was measured by applying the magnetic field parallel to the film plane, one must take complicated magnetization process of SRO into account.

B. Junction characteristics

The schematic cross section of the junction is shown in Fig. 2(a). The junction size was varied from 9 to 300 μm^2. Figure 2(b) shows the temperature dependence of resistance

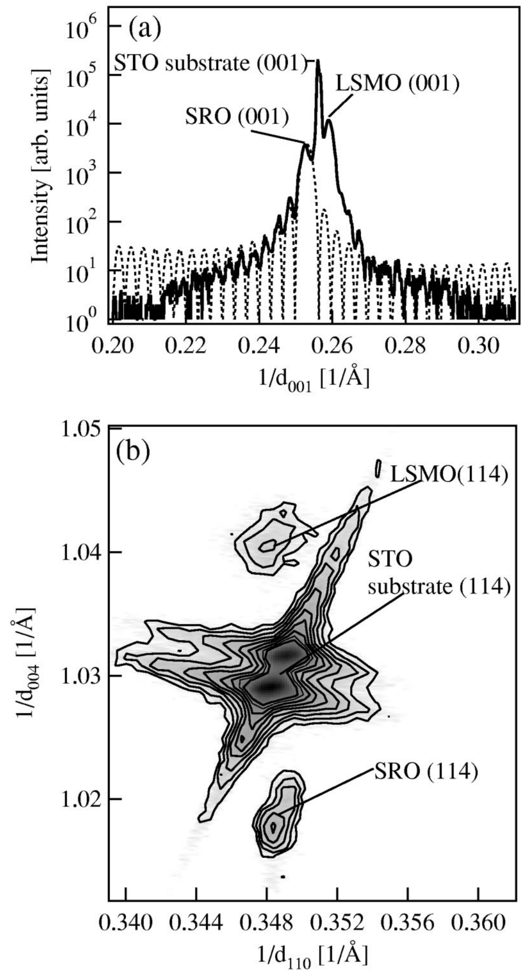

FIG. 1. X-ray diffraction of a LSMO(40 nm)/STO(8 unit cells)/ SRO(30 nm) heteroepitaxial thin film. (a) $2\theta-\theta$ scan for (001) peaks of perovskites. The out-of-plane lattice constants are 0.396 nm for SRO and 0.386 nm for LSMO layers. The dotted line is a simulated curve for a single layer of SRO film with a thickness of 30 nm, agreeing with the observed interference fringes. (b) Reciprocal space mapping for the (114) peaks of perovskites. Epitaxial films are coherently strained to the substrate. SRO is under compressive strain and LSMO is under tensile one.

for a tunnel junction (junction area of 3×20 μm^2) and the strip line lead (30×200 μm^2) for the bottom electrode. The bottom electrode strip line shows a metallic behavior and a kink at 140 K that corresponds to the ferromagnetic transition temperature T_C of SRO. The junction resistance is larger than the spread resistance of the bottom electrode by two orders of magnitude and stays constant at low temperatures. Figure 2(c) shows the bias voltage dependence of the junction current (on the left ordinate) and dynamic conductance dI/dV (on the right ordinate) for the junction at 10 K. The parabolic dependence of dI/dV on bias voltage indicates that the transport process for the junction is most likely the tunneling process. By fitting the characteristics to the theoretical formula,[16] a mean barrier height of 0.2~0.3 eV is deduced. In fact, such a small value as compared with the band gap of STO (3.2 eV) has been reported in literature[17,18] repeatedly for the junctions using a STO barrier. The origin is perhaps

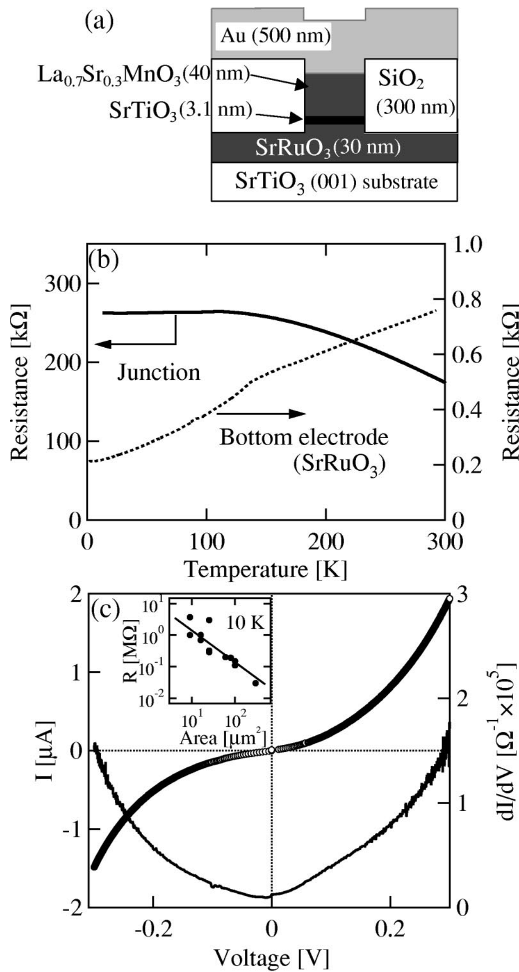

FIG. 2. (a) Cross-sectional schematic of the tunnel junction. (b) Temperature dependence of resistance for a $La_{0.7}Sr_{0.3}MnO_3$ /$SrTiO_3$ /$SrRuO_3$ tunnel junction with an area of 3×20 μm^2 (solid line, the left ordinate) and a bottom electrode strip line (dotted line, the right ordinate). (c) Bias voltage dependence of tunnel current (circles, the left ordinate) and dynamic conductance $dIdV$ (a solid line, the right ordinate) for the tunnel junction at 10 K. The inset shows the relationship between the resistance and junction area for the 12 junctions fabricated on the same chip.

due to the oxygen vacancy related subgap levels of STO, yet has never been clarified. The inset of Fig. 2(c) shows the relationship between junction resistance and junction area in a device chip. These are inversely proportional to each other and the yield against apparent leakage is pretty high ($\sim 80\%$). This is probably due to the smooth surface of the SRO layer grown in a step-flow mode. The TMR properties for these junctions as observed are quite reproducible and the representative ones are described below.

Figure 3(a) shows the magnetic-field dependence of magnetization (M-H curve) at 10 K for the single-layer films of LSMO (40 nm) and SRO (30 nm), and that for the LSMO (40 nm)/STO(8 unit cells)/SRO(30 nm) trilayer film before the device processing. Magnetic field was applied along the [100] direction (parallel to the film plane) in all the measurements. This axis is the magnetic easy axis for LSMO. By contrast, the magnetic easy axis of compressive epitaxial

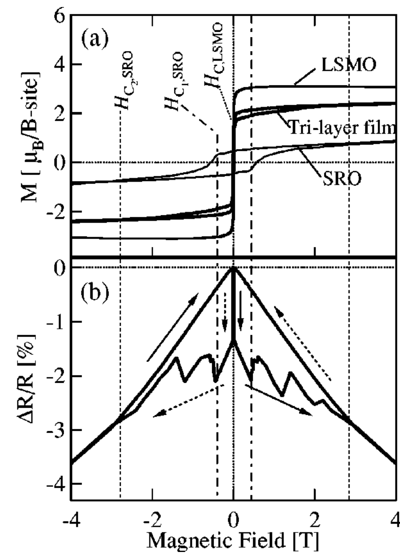

FIG. 3. (a) Magnetic-field dependence of magnetization for a 40-nm-thick $La_{0.7}Sr_{0.3}MnO_3$ film, 30 nm $SrRuO_3$ film, and $La_{0.7}Sr_{0.3}MnO_3$(40 nm)/$SrTiO_3$(8 unit cells)/$SrRuO_3$(30 nm) trilayer film measured at 10 K. (b) Magnetic-field dependence of $\Delta R/R$ at 10 K. The magnetic field was applied to the film plane.

strain of SRO is vertical to the film plane, giving rise to a large hysteresis up to 3 T at 10 K in the M-H curve as observed. Note that the magnetization is normalized by the formula unit of magnetic perovskite (i.e., except STO). As seen in Fig. 3(a), the magnetization for the tri-layer film can be regarded as the simple sum of those for LSMO and SRO, indicating no magnetic coupling between LSMO and SRO. There can be defined three characteristic magnetic fields as indicated in Fig. 3(a); coercive force of LSMO ($H_{c,LSMO}$ ~ 0.01 T), coercive force of SRO ($H_{c_1,SRO} \sim 0.4$ T) and the field ($H_{c_2,SRO} \sim 3$ T) at which the magnetization of SRO is aligned to the field direction (the magnetic hard axis).

Figure 3(b) shows the magnetic-field dependence of the TMR ($\Delta R/R$) at 10 K normalized by the junction resistance R at 0 T. Clear inverse TMR ($R_{AP} - R_P < 0$) is observed for all the junctions: $\Delta R/R$ abruptly decreases at $H_{c,LSMO}$ and increases above $H_{c_1,SRO}$ in a magnetic-field scan. Besides the anticipated inverse TMR response, two features are superimposed on the magnetic-field dependence of $\Delta R/R$; (1) stepwise increase of $\Delta R/R$ in a field range of $H_{c_1,SRO} < H < H_{c_2,SRO}$ and (2) almost linear decrease of $\Delta R/R$ as a function of magnetic field seen for the parallel magnetization branch during decreasing the magnetic field. Figure 4(c) shows the magnification of inverse TMR action in a low-magnetic-field region. The arrows in schematics represent the magnetization direction of the electrodes. Schematics of DOS for parallel and anti-parallel configurations are shown in Figs. 4(a) and 4(b), respectively, which will be described later. The resistance at the parallel configuration is higher than that at the anti-parallel one. At 0.01 T ($H_{c,LSMO}$), the magnetization configuration switches from parallel to anti-parallel, resulting in a sharp drop of $\Delta R/R$. The $\Delta R/R$ stays at a low resistance level up to 0.4 T ($H_{c_1,SRO}$) at which the

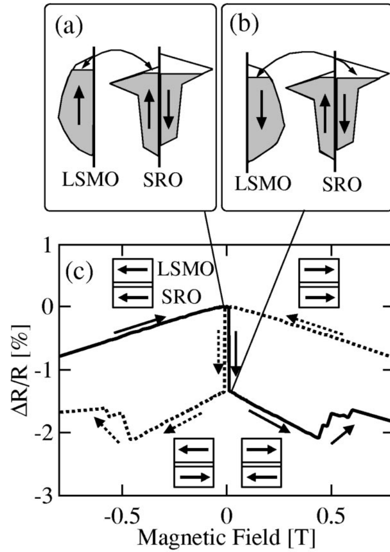

FIG. 4. (a) The band structures including spin polarization for the top $La_{0.7}Sr_{0.3}MnO_3$ and bottom $SrRuO_3$ electrodes in parallel magnetization configuration (high resistance state). (b) Those in antiparallel one (low resistance state). (c) Magnetic-field dependence of $\Delta R/R$ at 10 K in a low-field region.

magnetization direction of SRO starts to change from antiparallel to parallel. The stepwise increase of $\Delta R/R$ in a field range of $H_{c_1,SRO}<H<H_{c_2,SRO}$ cannot be correlated with rather smooth change of magnetization for the SRO film [Fig. 3(a)]. We presume that this stepwise change of $\Delta R/R$ is due to the magnetic domain-wall motion. The magnetic domain size of the SRO film was evaluated to be 0.1 $\sim$5 μm^2 by Lorentz mode transmission electron microscopy[19] and magnetic force microscopy[20] measurements. Because the domain size is comparable to the junction size, incremental domain wall motion or domain rotation during the field scan can be sensitively detected as the change of $\Delta R/R$ in such a small-area junction. On the contrary, the individual domain motion is likely smeared out on average in the magnetization measurement by SQUID for a specimen as large as 5×5 mm^2.

As mentioned above, this inverse TMR behavior indicates that the spin polarizations of LSMO and that of SRO are opposite. Figures 4(a) and 4(b) show schematic illustrations of DOS for parallel and antiparallel configurations, in which the DOS of LSMO is assumed as that of a half metal ($P=+100\%$) (Ref. 21) and the DOS of SRO refers to a result of theoretical calculation.[8] In the parallel configuration, the tunneling conductance is limited by the small DOS (or more precisely $N_\uparrow\times v_\uparrow^2$) near the Fermi level of up-spin band in SRO. In anti-parallel configuration, the tunneling conductance is enhanced by the large DOS ($N_\downarrow\times v_\downarrow^2$) near the Fermi level of down-spin band in SRO. Therefore, the observation of inverse TMR agrees qualitatively with the predicted band structures of the both compounds.

The temperature dependence of the TMR action is shown in Fig. 5(a). The abrupt change in $\Delta R/R$ at $H_{c,LSMO}$ decreases as the temperature increases. Contrary to previous reports for LSMO/I (e.g., STO)/LSMO magnetic tunnel

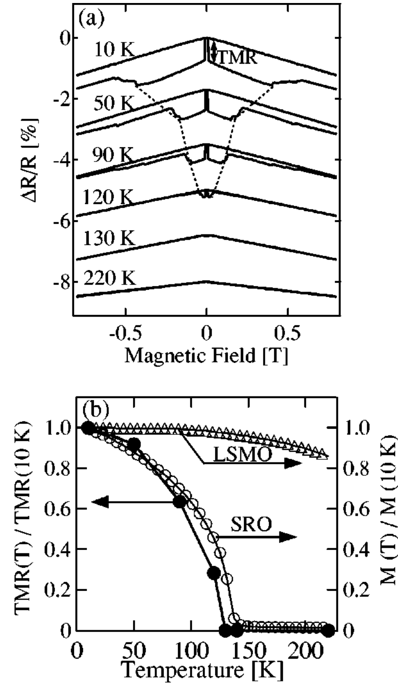

FIG. 5. (a) Magnetic-field dependence of $\Delta R/R$ at various temperatures. The traces are shifted vertically for clarity. The amplitude of tunnel magnetoresistance (TMR) is defined by the resistance jump at the coercive force of LSMO layer ($H_{c,LSMO}$) indicated by the arrow. The TMR action persists up to 120 K that is close to T_C of SRO layer (140 K). The temperature dependence of the switching field from parallel to antiparallel (a dotted line) agrees well with that of $H_{c_1,SRO}$. (b) Temperature dependence of the TMR amplitude normalized by the one at 10 K (●) for the tunnel junction (the left ordinate). Temperature dependence of the normalized magnetization (the right ordinate) is also given for $La_{0.7}Sr_{0.3}MnO_3$ (△) and $SrRuO_3$ (○) layers.

junctions where TMR action tends to vanish at a temperature far lower than T_C,[22–24] a finite inverse TMR hysteresis is observed clearly up to 120 K close to the T_C of SRO. This result indicates that the SRO/STO interface is robust in terms of spin polarization. The magnetic field at which $\Delta R/R$ starts to increase (indicated by dotted line) decreases as the temperature increases. The temperature dependence of this switching field coincides with that of the $H_{c_1,SRO}$, as expected. Figure 5(b) shows the temperature dependence of the TMR amplitude and magnetization of each layer normalized by the respective value at 10 K. The TMR amplitude is evaluated from $\Delta R/R$ at 0.01 T (a field just above $H_{c,LSMO}$) as indicated by a vertical arrow in Fig. 5(a). The value of the TMR amplitude is approximately proportional to the magnetization of the SRO layer. Since the magnetization of the LSMO layer is almost constant in this temperature range (10–140 K), this temperature dependence is governed by the temperature variation of the SRO spin polarization, in accord with Eq. (1).

The spin polarization P of SRO (P_{SRO}) is deduced from the present results as follows. We take the maximum value of TMR as being $-0.065(6.5\%)$ among all the junctions measured so far. The effective polarization of LSMO is deduced

from the experimental results of tunnel junctions as $P_{LSMO} = +0.80$ (+80%).[22,25] By simply putting these values into Eq. (1), we obtain P_{SRO} to be as small as -0.04 (-4%). Here, we note that the reduced magnetization of SRO ($\sim 0.4\ \mu_B/B$ site) at a field just above $H_{c,LSMO}$. This is because the magnetic field direction is along the magnetic hard axis of SRO. When we apply the field along the magnetic easy axis of SRO or high enough field along the magnetic hard axis, we obtain a saturated magnetization of $\sim 1.2\ \mu_B/B$ site for our films which agrees with the previous results. Therefore, we can consider that 1/3 of the SRO contributes to the $\Delta R/R$ and that the rest part of the SRO does nothing due to the cancellation. By multiplying a factor of 3, we obtain a rough estimate of $P_{SRO} = -0.12$ (-12%). This value is comparable to that (-9.5%) observed by tunneling spectroscopy for the SRO/STO/Al (superconductor) junction.[7]

The reduced spin polarization of LSMO at the LSMO/STO interface as assumed above is most likely due to the spin canting as discussed in a previous work.[10] This may also account for the linear background of TMR shown in Fig. 3(b): The linear background persists above T_C of SRO as seen in Fig. 5(a). Therefore, it should be correlated to the LSMO/STO interface. With the increase of magnetic field, the spin canting at the LSMO layer adjacent to STO is suppressed, yielding more perfect spin alignment. This may forward the tunneling transport of carriers between LSMO and SRO through STO, giving rise to the linear background in the R vs H curve. Such imperfect junctions as reduced spin polarization of LSMO due to spin canting and the possibility of pinholes or spin-independent conduction channels in the STO barrier limit the lower bound of spin polarization value of SRO (P_{SRO}) as -0.12 (-12%).

IV. CONCLUSION

We have grown epitaxially all-perovskite LSMO/STO/SRO trilayer films on STO (001) substrates and analyzed the tunnel junction characteristics. The junctions clearly show the inverse TMR action up to 120 K (close to T_C of SRO), indicating opposite sign of spin polarization in SRO and LSMO and the robust spin polarization at $SrRuO_3/SrTiO_3$ interface. Taking into account the reduced magnetization value of the SRO layer, we deduced a value of the lower bound of spin polarization in $SrRuO_3$ as $P_{SRO} = -0.12$ (-12%).

ACKNOWLEDGMENTS

This work was partly supported by New Energy and Industrial Technology Development Organization (NEDO) of Japan. One of the authors (K.S.T.) would like to thank the Japan Society for the Promotion of Science (JSPS) for financial support.

*Present address: DPMC, University of Geneva, 24 Quai Ernest Ansermet, 1211 Geneva 4, Switzerland.

[1] J.S. Moodera, L.R. Kinder, T.M. Wong, and R. Meservey, Phys. Rev. Lett. **74**, 3273 (1995).
[2] M. Julliere, Phys. Lett. **54A**, 225 (1975).
[3] I.I. Mazin, Phys. Rev. Lett. **83**, 1427 (1999).
[4] J.M.D. Teresa, A. Barthelemy, A. Fert, J.P. Contour, F. Montaigne, and P. Seneor, Science **286**, 507 (1999).
[5] M. Sharma, S.X. Wang, and J.H. Nickel, Phys. Rev. Lett. **82**, 616 (1999).
[6] K. Ghosh, S.B. Ogale, S.P. Pai, M. Robson, Eric Li, I. Jin, Zi-wen Dong, R.L. Greene, R. Ramesh, T. Venkatesan, and M. Johnson, Appl. Phys. Lett. **73**, 689 (1998).
[7] D.C. Worledge and T.H. Geballe, Phys. Rev. Lett. **85**, 5182 (2000).
[8] D.J. Singh, J. Appl. Phys. **79**, 4818 (1996).
[9] M. Kawasaki, K. Takahashi, T. Maeda, R. Tsuchiya, M. Shinohara, O. Ishiyama, T. Yonezawa, M. Yoshimoto, and H. Koinuma, Science **266**, 1504 (1994).
[10] M. Izumi, Y. Ogimoto, Y. Okimoto, T. Manako, P. Ahmet, K. Nakajima, T. Chikyow, M. Kawasaki, and Y. Tokura, Phys. Rev. B **64**, 064429 (2001).
[11] J.H. Neave, P.J. Dobson, and B.A. Joyse, Appl. Phys. Lett. **47**, 100 (1985).
[12] M. Lippmaa, N. Nakagawa, M. Kawasaki, S. Ohashi, Y. Inaguma, M. Itoh, and H. Koinuma, Appl. Phys. Lett. **74**, 3543 (1999).
[13] J. Choi, C.B. Eom, G. Rijnders, H. Rogalla, and D.H.A. Blank, Appl. Phys. Lett. **79**, 1447 (2001).
[14] M. Izumi, Y. Ogimoto, T. Manako, M. Kawasaki, and Y. Tokura, J. Phys. Soc. Jpn. **71**, 2621 (2002).
[15] L. Klein, J.S. Dodge, T.H. Geballe, A. Kapitulnik, A.F. Marshall, L. Antognazza, and K. Char, Appl. Phys. Lett. **66**, 2427 (1995).
[16] W.F. Brinkman, R.C. Dynes, and J.M. Rowell, J. Appl. Phys. **41**, 1915 (1970).
[17] T. Obata, T. Manako, Y. Shimakawa, and Y. Kubo, Appl. Phys. Lett. **74**, 290 (1999).
[18] M. Viret, M. Drouet, J. Nassar, J.P. Contour, C. Fermon, and A. Fert, Europhys. Lett. **39**, 545 (1997).
[19] L. Klein, Y. Kats, A.F. Marshall, J.W. Reiner, T.H. Geballe, M.R. Beasley, and A. Kapitulnik, Phys. Rev. Lett. **84**, 6090 (2000).
[20] T. Fukumura, K. S. Takahashi, and M. Kawasaki (unpublished).
[21] J.-H. Park, E. Vescovo, H.-J. Kim, C. Kwon, R. Ramesh, and T. Venkatesan, Phys. Rev. Lett. **81**, 1953 (1998).
[22] J.Z. Sun, W.J. Gallagher, P.R. Duncombe, L. Krusin-Elbaum, R.A. Altman, A. Gupta, Y. Lu, G.Q. Gong, and G. Xiao, Appl. Phys. Lett. **69**, 3266 (1996).
[23] M.-H. Jo, N.D. Mathur, N.K. Todd, and M.G. Blamire, Phys. Rev. B **61**, R14 905 (2000).
[24] J. O'Donnell, A.E. Andrus, S. Oh, E.V. Colla, and J.N. Eckstein, Appl. Phys. Lett. **76**, 1914 (2000).
[25] Y. Lu, X.W. Li, G.Q. Gong, G. Xiao, A. Gupta, P. Lecoeur, J.Z. Sun, Y.Y. Wang, and V.P. Dravid, Phys. Rev. B **54**, R8357 (1996).